JGR Atmospheres

RESEARCH ARTICLE
10.1029/2019JD032119

Impact of Cloud Ice Particle Size Uncertainty in a Climate Model and Implications for Future Satellite Missions

Yuan Wang[1,2], Hui Su[2], Jonathan H. Jiang[2], Feng Xu[3], and Yuk L. Yung[1,2]

[1]Division of Geological and Planetary Sciences, California Institute of Technology, Pasadena, CA, USA, [2]Jet Propulsion Laboratory, California Institute of Technology, Pasadena, CA, USA, [3]School of Meteorology, University of Oklahoma, Norman, OK, USA

Key Points:
- Climate mean state and climate sensitivity are sensitive to cloud ice particle size
- Ice particle size exerts larger climate impacts than that of falling snow with the same fractional changes
- A 33% reduction in R_{ei} uncertainty would lead to reductions in climate sensitivity and mean state uncertainty by 60% in CESM

Correspondence to:
Y. Wang,
yuan.wang@caltech.edu

Citation:
Wang, Y., Su, H., Jiang, J. H., Xu, F., & Yung, Y. L. (2020). Impact of cloud ice particle size uncertainty in a climate model and implications for future satellite missions. *Journal of Geophysical Research: Atmospheres*, *125*, e2019JD032119. https://doi.org/10.1029/2019JD032119

Received 26 NOV 2019
Accepted 5 MAR 2020
Accepted article online 10 MAR 2020

Abstract Ice particle size is pivotal to determining ice cloud radiative effect and precipitating rate. However, there is a lack of accurate ice particle effective radius (R_{ei}) observation on the global scale to constrain its representation in climate models. In support of future mission design, here we present a modeling assessment of the sensitivity of climate simulations to R_{ei} and quantify the impact of the proposed mission concept on reducing the uncertainty in climate sensitivity. We perturb the parameters pertaining to ice fall speed parameter and R_{ei} in radiation scheme, respectively, in National Center for Atmospheric Research CESM1 model with a slab ocean configuration. The model sensitivity experiments show that a settling velocity increase due to a larger R_{ei} results in a longwave cooling dominating over a shortwave warming, a global mean surface temperature decrease, and precipitation suppression. A similar competition between longwave and shortwave cloud forcing changes also exists when perturbing R_{ei} in the radiation scheme. Linearity generally holds for the climate response for R_{ei} related parameters. When perturbing falling snow particle size (R_{es}) in a similar way, we find much less sensitivity of climate responses. Our quadrupling CO_2 experiments with different parameter settings reveal that R_{ei} and R_{es} can account for changes in climate sensitivity significantly from +12.3% to −6.2%. By reducing the uncertainty ranges of R_{ei} and R_{es} from a factor of 2 to ±25%, a future satellite mission under design is expected to improve the climate state simulations and reduce the climate sensitivity uncertainty pertaining to ice particle size by approximately 60%. Our results highlight the importance of better observational constraints on R_{ei} by satellite missions.

1. Motivation and Background

Ice clouds are present in the upper troposphere mainly in three forms: in situ formed cirrus, deep convection tower, and convection detrained anvil. Global coverage of ice clouds is about 40%, while in the tropics, ice cloud fraction is close to 70% (Stubenrauch et al., 2013). By trapping infrared radiation and scattering solar radiation, ice clouds can either warm or cool the Earth surface (Yang et al., 2015). Over the tropics, radiative warming arising from high-altitude ice cloud can be as large as +80 W m^{-2} at the top of atmosphere (Stephens et al., 2002). Hence, radiative properties of ice clouds are crucial in regulating the Earth's radiation and energy balance and altering the climate feedbacks and climate sensitivity (e.g., Sanderson et al., 2007; Schiro et al., 2019; Su et al., 2017). Ice particle size is a critical physical property which is closely related with the cross section for longwave absorption and efficiency of shortwave scattering (Fu & Liou, 1993; Liu et al., 2014). Moreover, via cloud microphysical processes (Eidhammer et al., 2014), ice particle size largely determines precipitation formation and surface precipitation rate in the mixed phase and deep convective clouds. Specifically, it controls ice particle falling speed and alters the efficiency of several microphysics, such as collection of cloud droplets, conversion of ice to snow, and graupel deposition/sublimation (Li et al., 2008). Overall, ice particle size can be a useful index to characterize convective strength, high-level moisture content, and even different ice nucleation pathways (Zhao et al., 2018, 2019).

The Earth's NexT-generation ICE (ENTICE) is a future satellite mission concept, aiming to provide more accurate retrieval of ice particle size than existing satellites (Jiang et al., 2017, 2019). It combines a 15-channel passive microwave radiometer and profiling W-band cloud radar. The microwave radiometer suite has high sensitivity to a wide range of ice water content (IWC) profiles spanning from thin cirrus to deep convective ice (above the melting layer). An addition of the 850 GHz frequency in ENTICE increases the sensitivity of the microwave radiometers to ice clouds with optical depth larger than 0.1. Note that

this sensitivity also depends on the IWC and particle size. The cloud radar supplements the radiometer by better resolving the vertical structures of cloud mass and particle size with an improved vertical resolution of 0.5 km. Therefore, a future mission like ENTICE is expected to reduce the uncertainty in the ice particle size and IWC to less than 25% (Jiang et al., 2019). A consequent question related with this uncertainty reduction is what the corresponding climatic significance is. Since the true values of ice particle size remain unknown on the global spatial scale and decadal time scale due to the present imperfect observations, we have to use a state-of-the-art climate simulation as a "nature run" and then explore climate sensitivity changes owing to any change in the targeted cloud properties. The similar strategy has been widely used in the Observing System Simulation Experiment that aims to estimate impacts of proposed designs of new satellites in a modeling framework (Errico et al., 2013).

Ice particle size in current general circulation models (GCMs) remains largely unconstrained. Previous modeling studies revealed that altered cloud radiative forcing following ice particle size perturbations can modulate large-scale circulation and precipitation (Muri et al., 2014) and influence climate sensitivity (Sanderson et al., 2007). This study aims to provide a quantitative answer for how climate simulation and projection can be affected, if we calibrate ice particle size in GCM by future satellite mission formulation like ENTICE. We perform a series of parameter perturbation experiments in the National Center for Atmospheric Research (NCAR) Community Earth System Model (CESM) and explore the sensitivity of climate mean state as well as future climate change in response to ice particle size variations in a range consistent with the ENTICE measurement uncertainty. In this study, we focus on the two major aspects of the ice particle size influence: spatial distribution and radiative effects of ice particles.

2. Methodology

2.1. Model Description

CESM version 1.2.2 is employed in this study. The atmospheric component CAM5.3 explicitly considers ice cloud microphysics for grid-scale stratiform cloud using a two-moment microphysical scheme (Gettelman et al., 2008). A gamma size distribution is assumed for ice crystals, and the effective radius of ice particle (R_{ei}) is a function of ice mass mixing ratio and number concentration, two prognostic variables in the model. Detrained ice from the deep convection parameterization (Zhang & Mcfarlane, 1995) is added to the ice mass and number budget before the microphysics call in each time step. Since only ice mass mixing ratio is predicted in the convection parameterization, a fixed convection-detrained ice particle radius (25 μm) is used to convert mass to number concentration accordingly, which is also a tunable parameter in CAM5. After all other cloud physical processes are computed, the Rapid Radiative Transfer Model for GCMs (RRTMG) is called and R_{ei} derived from the current ice number, and mass concentrations are used to compute the ice cloud optical properties.

To diagnose climate sensitivity in a computationally efficient way, the slab ocean configuration of CESM is adopted in the present study. The ocean model interacts with other components in CESM but only as one thermal layer with prescribed ocean circulation (Wang et al., 2017). The model experiments start from the "PI-control" with preindustrial emission conditions. All the simulations are found to reach an equilibrium state within 30 years (the top-of-atmosphere [TOA] net radiation flux close to 0 and surface temperature stabilized), and our analyses are based on the averages of the last 10 years. Note that for those parameter-perturbed experiments, the new equilibrium states are slightly different with the present-day climate in terms of the TOA atmospheric radiative fluxes and/or global mean surface temperature, but the responses in the atmospheric states are still valuable to reflect the importance of certain model parameters, as done in many previous modeling works (Qian et al., 2015; Schiro et al., 2019; Tan et al., 2016). We choose not to tune the TOA radiative fluxes back to the observational values, because such a tuning can exert marked influence on the model's climate sensitivity and overshadow the effects of parameter perturbation in this study.

2.2. Parameter-Perturbation Experiment Design

As R_{ei} is a diagnostic variable in CAM5, we can only alter its value and assess its influence in the model components where R_{ei} is used. In the present study, we separately perturb the R_{ei} related parameters in the ice fall speed calculation and in the radiation transfer model. Ice particle fall speed is parameterized as $Vi = ai \times$

Table 1
Numerical Experiment Design

Experiment purpose	Parameter perturbed	Fractional change	Uncertainty range	Integration time
To assess R_{ei} influence on ice cloud variability	ai in R_{ei} fall speed parameterization	−50% +100%	CESM default	30 years
		−25% +25%	ENTICE	30 years
To assess R_{ei} influence in radiation	RR_{ei} in radiation transfer	−50% +100%	CESM default	30 years
		−25% +25%	ENTICE	30 years
To assess R_{es} influence	as and RR_{es}	All 8 exp. above	CESM/ENTICE	30 years
To quantify climate sensitivity	$4 \times [CO_2]$	All 16 exp. above	CESM/ENTICE	30 years

$D_{ei}{}^{bi}$, where $D_{ei} = 2 \times R_{ei}$. Since bi is 1, any perturbation on the fall speed parameter ai can be translated into the same fractional changes in R_{ei}. The default value of ai is 700, but the model suggested range is 350–1,400, corresponding to −50% and +200% error range. Considering ENTICE would have a ±25% uncertainty range, we then perturbed ai to 50%, 75%, 125%, and 200% of its default value. Note that since the true value of R_{ei} is unknown, we use the model's current simulation of R_{ei} as the base value.

In RRTMG radiation scheme, we directly alter the R_{ei} value as the input to radiation (RR_{ei}). Note that such an alteration is only applied to the radiation calculation. We found that changing RR_{ei} exerts negligible effect on the ice mass and number concentrations, so the proposed enhanced turbulence and cirrus cloud vertical development by in-cloud radiative heating (Hartmann et al., 2018) does not occur in such a large-scale model. The same magnitude of perturbations was applied to RR_{ei} in the radiation scheme.

In the CAM5 physics, ice and snow are represented in two separated size spectra, each of which can be used to calculate their own mass mixing ratio and number concentration. The difference lies in that the snow budget are treated diagnostically (not carried over to the next time step). The conversion between ice and snow includes autoconversion from ice to snow and accretion of ice by snow. The radiative effect of falling snow is explicitly considered in CAM5. Some previous studies suggested the paramount importance of the snow radiative effect in reproducing the present-day radiative heating profiles and even polar sea ice in GCM (Li et al., 2016, 2017). Therefore, we repeat all the parameter perturbation experiments for the particle size of falling snow (R_{es}) in the same way with the those for R_{ei}. The quadrupling-CO_2 experiments were conducted to estimate climate sensitivity. Total 32 perturbation experiments are performed in this study, as summarized in Table 1.

3. Scientific Findings

3.1. Evaluation of Ice Cloud Properties Simulated by CESM

Ice cloud optical thickness (COT) and R_{ei} near cloud top from the Moderate Resolution Imaging Spectroradiometer (MODIS) Collection 6 Level 3 are used to evaluate the CESM simulated ice properties. Three-year Atmospheric Model Intercomparison Project style simulations are conducted since 2006, and the results in year 2008 are compared against MODIS. As shown in Figures 1a and 1b, the model shows generally good agreement with MODIS in the geospatial distribution of COT. It reproduces the large COT over the Intertropical Convergence Zone (ITCZ), storm tracks, and Asian monsoon regions. The major discrepancy occurs over Arctic and Antarctic. The model tends to overestimate COT over continents but underestimate it over the subtropical subsidence regions. The tropical mean COT in the model is 12.8 which is close to the MODIS observation 13.3. For R_{ei}, both MODIS and CESM show that the larger R_{ei} occurs over tropical convective regions. However, with respect to the magnitude, R_{ei} from MODIS is significantly larger than the model prediction. Here we average R_{ei} over all ice cloud layers in Figure 2d. Even though we use the maximal R_{ei} from all layers, the underprediction still exists.

Such a R_{ei} discrepancy can be caused by the known large biases in model R_{ei} as well as the uncertainty in satellite retrievals (Lai et al., 2019). MODIS cannot clearly distinguish ice and snow defined in the model, as long as

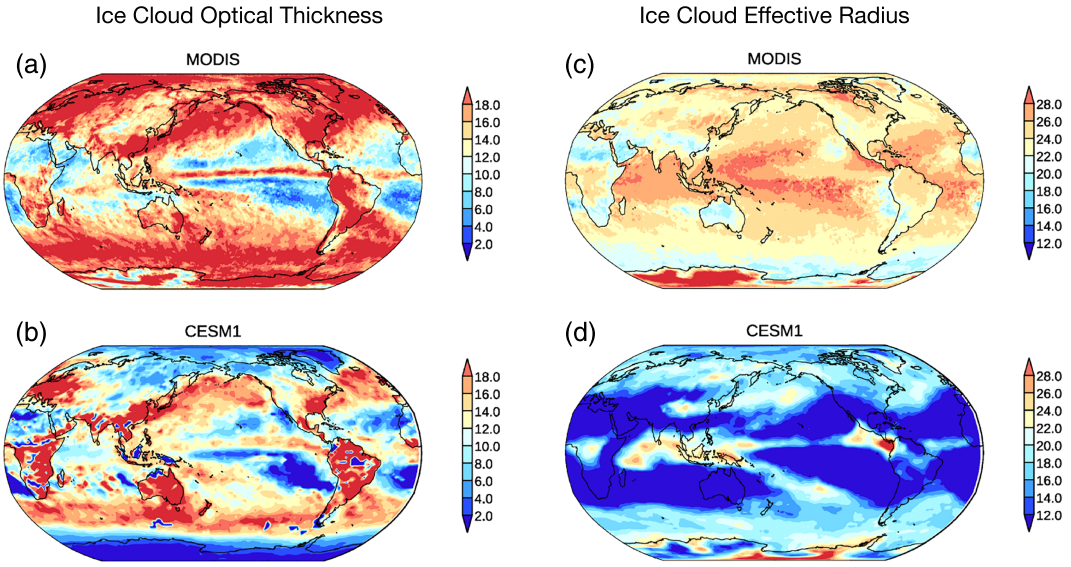

Figure 1. Comparison of cloud optical thickness (a, b) and ice particle effective radius (c, d) between MODIS and CESM.

they are floated near the cloud top. Also, different sensors using different wavelength bands can easily cause a 5–10 μm difference in retrieved R_{ei}, like MODIS versus Atmospheric Infrared Sounder (Kahn et al., 2015). Over the tropical deep convective regions, Wang et al. (2019) showed that due to the strong vertical heterogeneity of ice particles, there could be a 50% negative bias in both ice water path (IWP) and column averaged R_{ei} in MODIS monthly (L3) product for deep convective clouds. We also examine the CESM results using the MODIS satellite simulator from the Cloud Feedback Model Intercomparison Project Observation Simulator Package. Their comparison with the MODIS retrieval turns out to be even worse, as there is no agreement between the model and MODIS in either spatial distribution or its magnitude (not shown).

3.2. Atmospheric Changes by Perturbing Ice Size-Related Parameters

Larger ice particles tend to settle faster, and then ice cloud amount is expected to reduce in the upper troposphere. Figure 2 shows that the response of cloud properties to the *ai* perturbations is monotonic; that is, a larger response follows a larger perturbation. When we enlarge R_{ei} and increase ice settling velocity, a significant reduction of IWC that occurs near 200 hPa is found (Figure 2a). Consequently, there is a slight increase in IWC between 300 and 400 hPa but with a much smaller magnitude. Hence, the column-integrated ice water path is reduced when *ai* (ice fall speed) increases. Meanwhile, the liquid cloud content is found to be significantly decreased within the boundary layer as well as above 500 hPa (Figure 2b). It may be explained by the suppressed surface moisture flux and reduced water vapor content with an increase in *ai* (Figure 3d). The signs of total cloud fraction changes in vertical profile are generally consistent with those

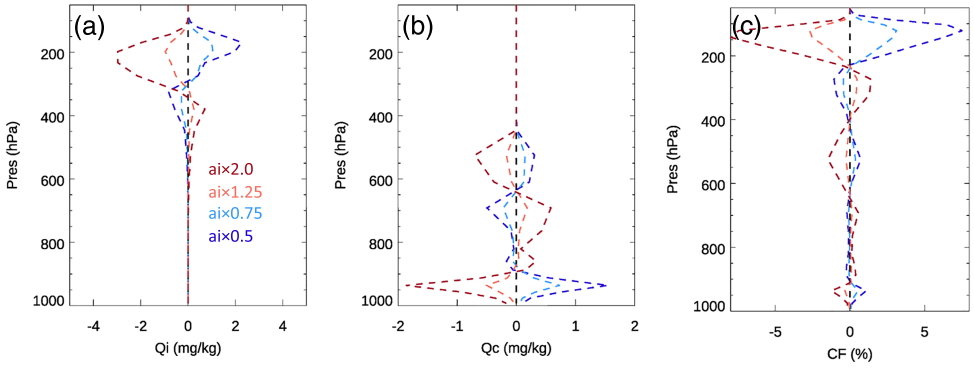

Figure 2. Comparison of changes in (a) ice water content, (b) liquid water content, and (c) cloud fraction amount over the tropics (20°S to 20°N) for different *ai* perturbation experiments.

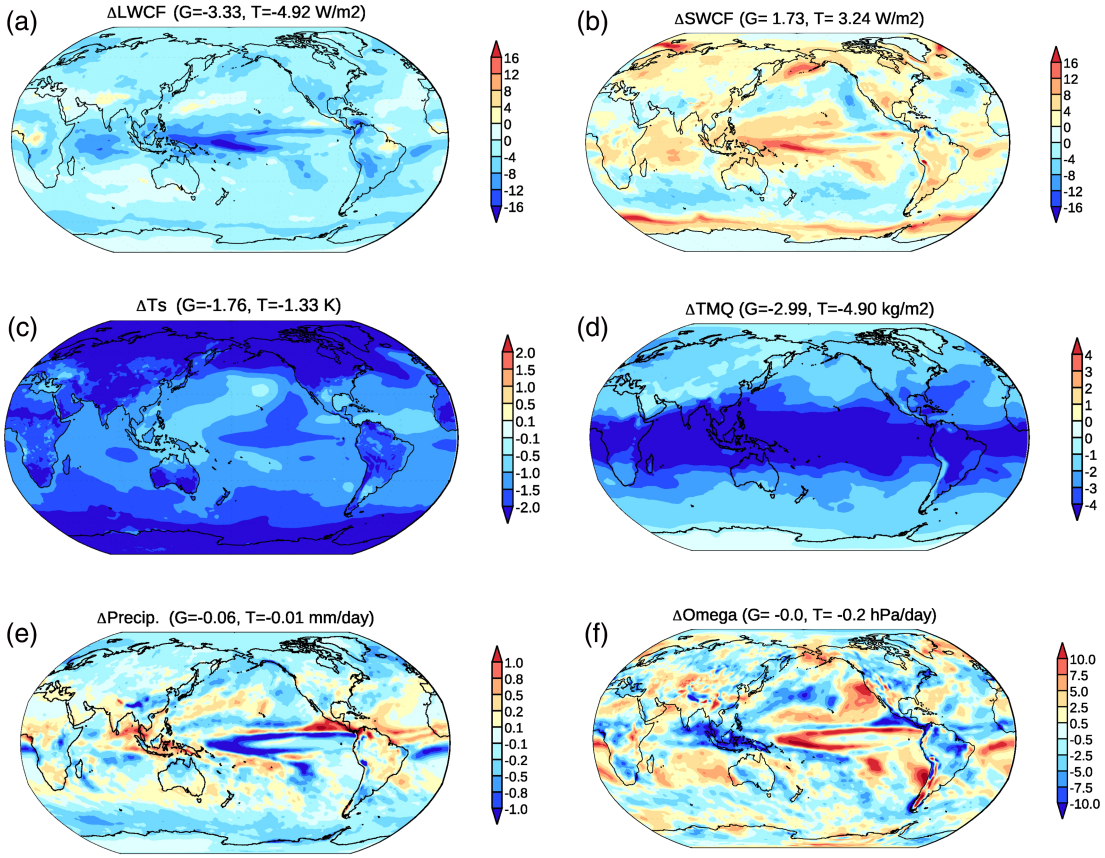

Figure 3. Differences of (a) longwave cloud radiative forcing, (b) shortwave radiative forcing, (c) surface temperature, (d) column-integrated water vapor, (e) total precipitation, and (f) vertical motion at 500 hPa between the 2 × *ai* and control run.

in ice and liquid water amount (Figure 2c). The disproportionate changes between liquid water content and fraction reflect the one caveat in CAM5, that is, the separate parameterizations of cloud microphysics and macrophysics.

We further analyze the differences in regional radiation budget and precipitation pattern between the doubling *ai* and the control runs. The IWC reduction owing to the R_{ei} increase results in the longwave cloud radiative forcing (LWCF) decreases as the outgoing longwave radiation increases (Figure 3a). Most of the changes occur in the equatorial tropics, presumably due to the large abundance of convection-detrained ice cloud over that region. Shortwave cloud radiative forcings (SWCF, negative values) exhibit more complicated spatial patterns (Figure 3b). Other than the SWCF reduction over the equatorial tropics, the subtropical and midlatitude regions (especially the Southern Ocean) receive larger SWCF, indicating more cloud amount. A further examination of air temperature and relative humidity reveal a positive cloud feedback over those regions, that is, more liquid cloud fraction and water content following the regional temperature decrease. By doubling *ai*, LWCF is reduced by 3.33 W m^{-2} globally and by 4.92 W m^{-2} over the tropics. In contrast, both global and tropical mean SWCF become more positive (Figure 3b) following the reduction of both high and low clouds. As for the net cloud forcing, the LWCF changes still dominate, and there is a net loss of radiative energy into the Earth system. The previous CAM3 ice perturbation experiment which imposed different ice size distributions (Mitchell et al., 2008) showed the same-sign changes in LWCF and SWCF individually but with a net positive forcing when ice particle size increases due to the larger SWCF. Hence, the global surface temperature (T_s) shows a significant reduction (Figure 3c), about −1.76 K with doubling *ai*. The spatial patterns of LWCF and SWCF changes resemble the global distribution of ice cloud. In contrast, the spatial pattern of T_s features the polar amplification, that is, much larger T_s variations in the higher-latitude region due to the sea ice feedback. Besides T_s, other variable changes are more evident in the tropics. The precipitation is decreased overall but with complex regional features (Figure 3d).

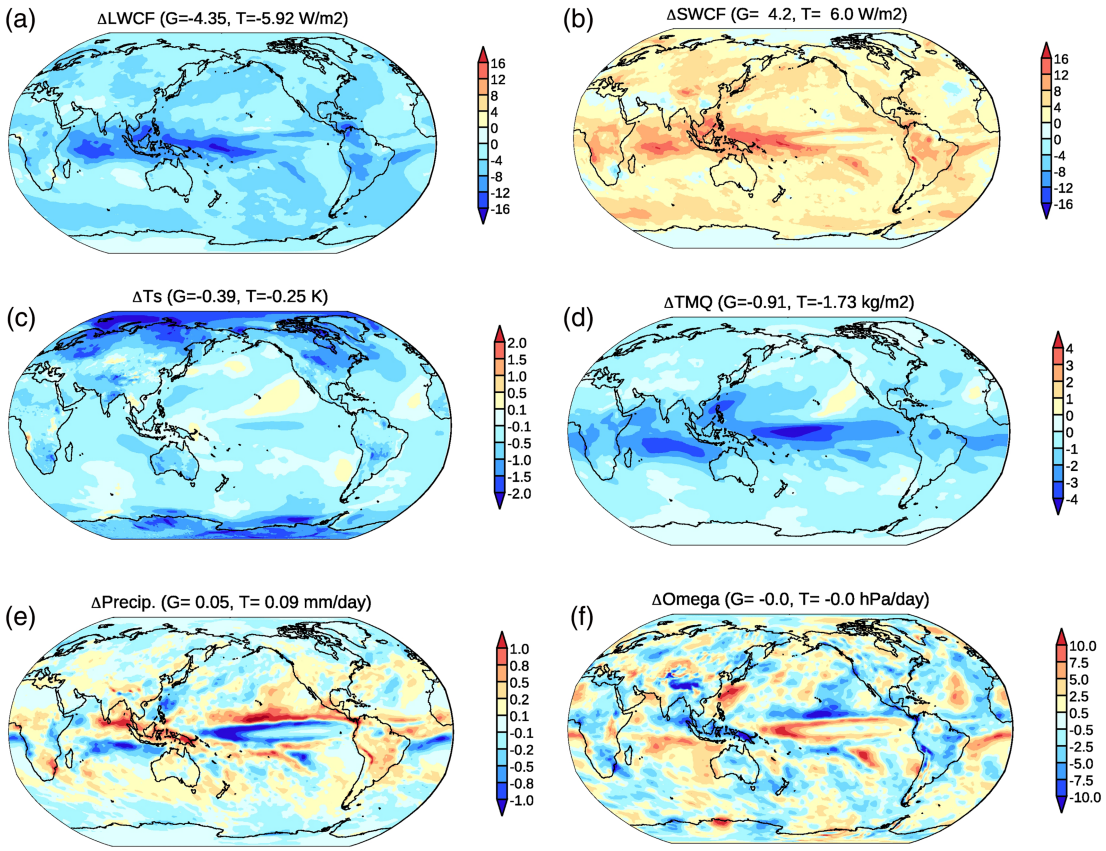

Figure 4. Atmospheric responses to doubling RR_{ei} in CESM, including (a) longwave cloud forcing, (b) shortwave cloud forcing, (c) surface temperature, (d) total column water vapor, (e) total precipitation, and (f) vertical motion at 500 hPa.

One prominent feature is the significant enhancement/reduction of precipitation over the north/south branch of the ITCZ. The reason for such ITCZ changes by *ai* will be explored later with other perturbation experiments. Another important feature in the precipitation change is the seesaw pattern in the Indo-Pacific Warm Pool, with a stronger precipitation reduction/enhancement in the western/eastern part of the region. The precipitation changes are well correlated with those in the large-scale ascending motion ($\text{Omega}_{500\text{hPa}}$, Figure 3f), indicating a dominant role of atmospheric circulations in affecting the spatial pattern of precipitation.

Ice cloud fraction, IWC, and ice particle size are important factors for ice cloud interference with the atmospheric radiation transfer. With an increase in RR_{ei}, both longwave and shortwave cloud radiative forcing are largely reduced (Figures 4a and 4b). Since we do not perturb the total ice water amount used in the radiation scheme, the larger ice crystal also means fewer ice number concentration, leading to a reduction in the effective cross section for the same amount of ice cloud. Hence, longwave absorption by the ice clouds is suppressed. Meanwhile, the fewer but larger ice particles are also less effective in scattering shortwave radiation. Overall, the changes in LWCF and SWCF are canceled out, leaving T_s largely unchanged, especially over the tropics (Figure 4c). Similar to doubling of *ai*, doubling of RR_{ei} induces an increase in water vapor over the tropics but with only one third of magnitude. Interestingly, the surface precipitation is quite sensitive in the RR_{ei} perturbation experiments. A more prominent northward shift of ITCZ can be found in the doubling-RR_{ei} experiment (Figure 4e). The distinctive changes between surface precipitation and temperature imply a rather loose connection between those two at local scale. Instead, the changes in large-scale circulations (Figure 4f) following the atmospheric energy perturbation are more relevant in explaining the precipitation changes.

A shift of the ITCZ location accompanies atmospheric energy difference between two hemispheres. A larger moist static energy deficit (surplus) in the Southern (Northern) Hemisphere will require an energy transport

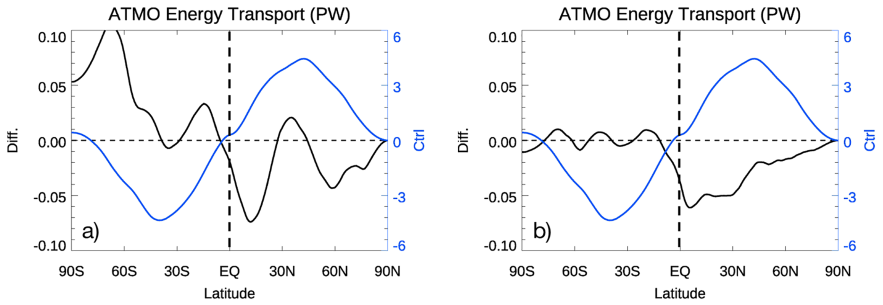

Figure 5. The climatology and anomalies of atmospheric energy transport in doubling *ai* (a) and doubling RR_{ei} (b) experiments.

across the equator from north to south (Schneider et al., 2014). By examining the meridional atmospheric heat transport (meridionally integrated atmospheric heat from the north pole to certain latitude), we find the enhanced equatorial atmospheric energy flow by doubling *ai* or RR_{ei} (Figure 5). Compared with doubling of *ai*, doubling of RR_{ei} leads to a larger energy surplus in the atmosphere of Northern Hemisphere but a smaller change in the Southern Hemisphere. Consequently, there is a much stronger southward atmospheric energy flow, corresponding to a more significant ITCZ southward shift with the doubling of RR_{ei}. One major implication is that better observational constraints on R_{ei} at the regional scale by future satellite missions can improve the regional energy balance and global circulation and precipitation patterns.

The possible influence of the observational constraints on R_{ei} by ENTICE can be assessed by comparing different *ai* or RR_{ei} perturbation experiments. In Figure 6, the reductions of the ranges/spreads from the error bars to the error boxes for each quantity correspond to the narrowing down of the model uncertain by imposing the R_{ei} constraints enabled by ENTICE. For the constraint via fall speed, the improvement rate ($1 - \text{range}_{\text{ENTICE}}/\text{range}_{\text{Default}}$) is consistent among LWCF, SWCF, T_s, and precipitation, corresponding to 62.7%, 61.0%, 65.2%, and 70.0%, respectively. Those large improvement rates suggest the significant impacts of observational constraint of fall speed on the climate simulations. For the R_{ei} influence on radiation, due to the large cancelation of LWCF and SWCF changes, the surface temperature remains insensitive. Except for T_s, LWCF, SWCF, and precipitation exhibit similar improvement rates, ranging from 62–65%. Considering those two parameters (*ai* and RR_{ei}) working in the same direction, we conclude that a better constraint on R_{ei} by ENTICE can benefit the surface temperature simulation mainly through a more realistic representation of ice fall speed and related ice cloud lifetime. Both parameters are relevant to the precipitation simulation.

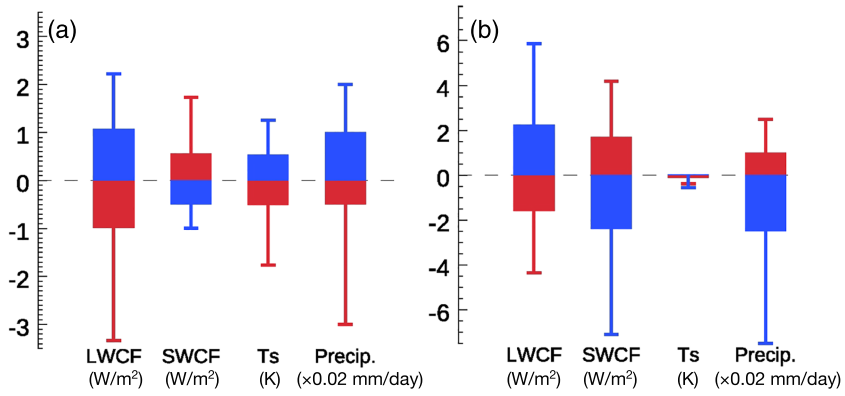

Figure 6. Changes in longwave cloud radiative forcing, shortwave radiative forcing, surface temperature, and total surface precipitation between perturbation and control runs. (a) For *ai* perturbation and (b) for RR_{ei} perturbation. Red color indicates the influence from R_{ei} increase, while blue color indicates the influence from R_{ei} decrease. The error bars correspond to the current model parameter ranges ($0.5–2.0 \times ai$), and the error boxes correspond to the ENTICE constrained parameter range ($0.75–1.25 \times ai$). Blue and red colors indicate parameter decrease and increase, respectively.

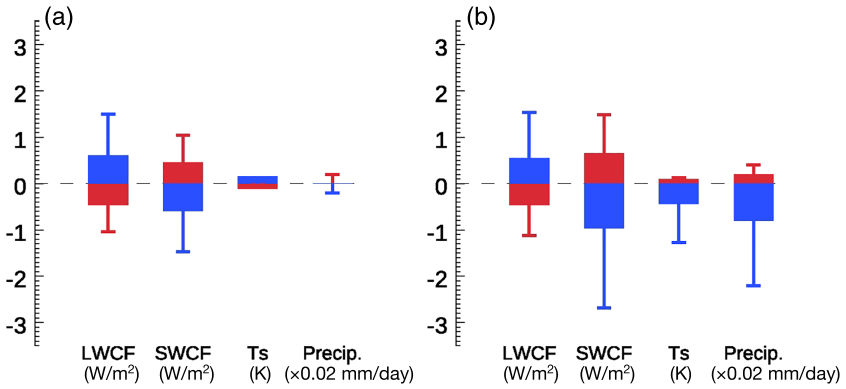

Figure 7. The same as Figure 6 but for snow particle size. (a) *as* and (b) RR_{es} perturbations.

3.3. Atmospheric Changes by Perturbing Snow Size Parameters

The upper limit of particle size detection range for a future mission like ENTICE can be close to 1,000 μm. Hence, it is interesting to know to what extent the expected reduction in the uncertain range of R_{es} by ENTICE can improve the climate simulations. We perform the same sensitivity runs by perturbing snow fall speed parameter (*as*) and snow particle size in the radiation transfer scheme (RR_{es}). Figure 7 shows that there is much smaller variation in those snow crystal size-related experiments than that in the ice-related ones. Specifically, *as*-induced changes in LWCF and SWCF are only about half of those from *ai*, and they largely cancel out with each other, rendering the total cloud forcing change diminished. This leads to little changes in surface temperature and precipitation even with the changing snow fall speed. Reducing RR_{es} in the radiation leads to a significant shortwave cooling, followed by a global reduction of T_s and precipitation. Strong nonlinearity is found for both T_s and precipitation responses, as the same fractional decrease in RR_{es} ends up with larger changes in T_s and precipitation, compared to those with the same fractional increase. Owing to the future satellite missions, the climate improvement rates for RR_{es} are quite consistent, about 61%. Considering the overall weak sensitivity to the R_{es}, the impact of ENTICE arising from tighter snow size constraints is likely to be small accordingly.

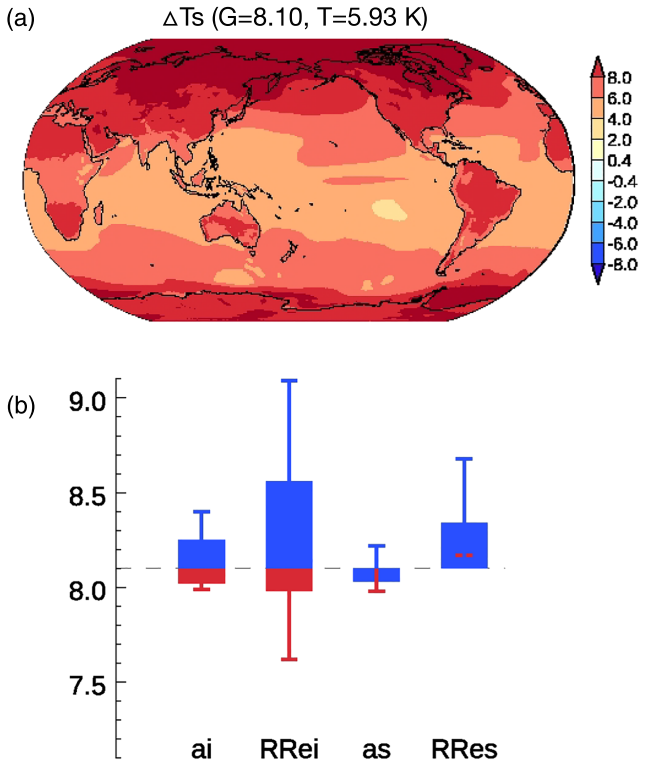

Figure 8. Surface temperature changes by quadrupling CO_2 under different ice and snow particle size. (a) The spatial map of T_s changes from the model default setting and (b) with changes in T_s owing to different parameters related with ice and snow particle size.

3.4. Influence of Ice/Snow Particle Size on Climate Sensitivity

The Earth's climate sensitivity is defined as the global mean surface temperature increase caused by a doubling of CO_2 concentration at the preindustrial level in the atmosphere. Here we quadruple CO_2 concentration and find an increase of 8.1 K in T_s in CESM, corresponding to a 4.05 K climate sensitivity for this model. From the spatial map of T_s change (Figure 8a), the polar amplification is evident. Under different R_{ei} and R_{es} parameter configurations, the model's climate sensitivity is more susceptible to RR_{ei} and RR_{es} than to *ai* and *as*. Among them, RR_{ei} exhibits the largest influence on climate sensitivity, resulting in a relative change from +12.3% to −6.2%. ENTICE can narrow down the uncertain range by 60% via constraining RR_{ei}. For the other three parameters, ENTICE can contribute to a varying improvement rate (43.9–112.5%).

The mean surface precipitation change is 0.46 mm day^{-1} when CO_2 is quadrupled, corresponding to a 1.9% K^{-1} hydrological sensitivity. The majority of the regions in the Northern Hemisphere experience an intensified hydrological cycle, the same as the Southern Ocean (Figure 9a). The southern branch of ITCZ has the most significant

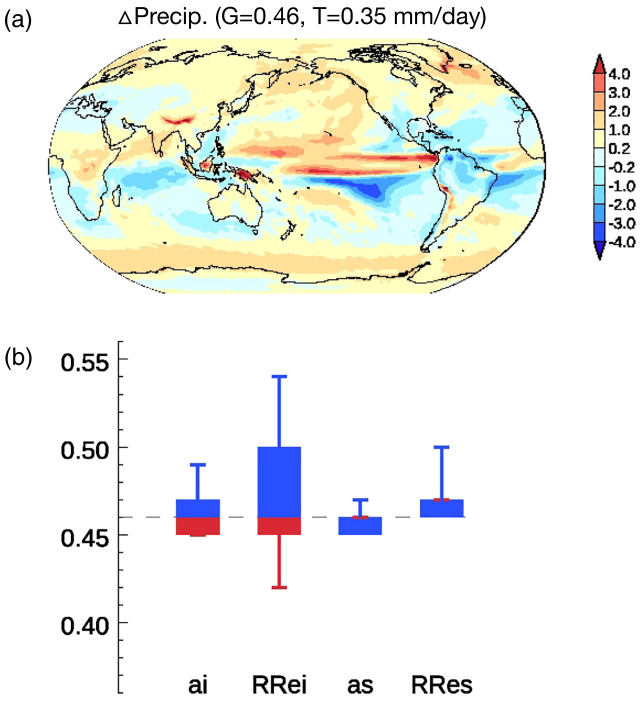

Figure 9. The same as Figure 8 but for the hydrological sensitivity.

reduction of precipitation, in contrast to the northern branch, corroborating the notion about the southward shift of ITCZ under global warming. In comparison of different ice/snow size parameter settings (Figure 9(b)), RR_{ei} exhibits the largest influence on hydrological sensitivity, resulting in a relative change from +17.4% to −8.7%. Similar to the impact on climate sensitivity, ENTICE can reduce the uncertainty arising from RR_{ei} in the hydrological sensitivity by 58%. Strong nonlinearity of hydrological sensitivity is found for the snow size-related parameters.

4. Conclusion and Discussion

Owing to the lack of accurate observations on the global scale, ice particle size in global climate models remains largely unconstrained. Hence, there is a pressing need to better understand the role of ice clouds particle size variations in climate change. A future satellite mission concept ENTICE which combines multifrequency passive sensors and vertical profiling active ones shows great potential in constraining the ice particle effective radius within 25% uncertain range. In this study, we adopt a modeling platform, NCAR CESM with a slab model, to assess the potential climatic influence of the well-constrained ice particle size.

We first show that there is no agreement on the magnitudes of in-cloud ice particle effective radius (R_{ei}) between CESM and MODIS-type passive satellite observations. It provides us the rationale of perturbing R_{ei} related parameters to different magnitudes. To study the R_{ei} effect on ice cloud vertical distribution and lifetime as well as their radiative effects, we target on ice fall speed parameter (ai) and R_{ei} in cloud radiation transfer (RR_{ei}), two independent variables in the model. Four levels of perturbation are conducted for each parameter, two of which correspond to the uncertainty range of ENTICE. For ai, it is found that the changes in longwave cloud forcing are larger than its shortwave cloud forcing, so a larger R_{ei} results in a lower ice cloud peak and a net radiative cooling on the surface. The surface precipitation over the ITCZ shows the largest sensitivity to ice parameter perturbations, and its pattern is determined by the interhemispheric energy imbalance as well as large-scale circulation change. For RR_{ei} perturbation, surface temperature remains largely unchanged owing to the cancelation of LWCF and SWCF stemming from radiative properties changes. In contrast, surface precipitation exhibits much larger sensitivity, due to the larger energy imbalance spatially. Strong linearity is generally found for the climate response for R_{ei} related parameters. We repeat the similar parameter perturbation experiments but for snow particle size (R_{es}) and find much less sensitivity in climate mean states. Different from R_{ei}, significant nonlinearity in T_s and precipitation responses is found for R_{es}-related parameter, especially for RR_{es}. By confining the uncertainty range in R_{ei} and R_{es} to ±25%, ENTICE is expected to improve climate mean state simulation by 60% roughly.

Climate sensitivity is estimated by quadrupling CO_2 concentration in the slab ocean setup. All the possible changes in ice-/snow-related parameters can cause a relative change of climate sensitivity from +12.3% to −6.2%. RR_{ei} is found to impose the largest influence on the climate sensitivity among all perturbed parameters. A future satellite mission like ENTICE is expected to better constrain the modeled climate sensitivity by 60%. The role of different ice/snow parameters in affecting the hydrological sensitivity resembles that of the climate sensitivity above.

We acknowledge that the present study is based on one climate model, and the quantitative results may differ for different models. Note that the latest version of CESM model (CESM2) has reported a higher climate sensitivity of about +5.3 K (Gettelman et al., 2019), so one of our future works is to explore the role of R_{ei} in affecting such a climate sensitivity. Also, we do not explore the possible influence of R_{ei} or R_{es} on individual microphysical processes in this study, since it requires comprehensive perturbations on all relevant parameters and processes (deposition, riming, ice accretion, snow autoconversion, and so on) that are planned for a future study.

Acknowledgments

This work was conducted at the NASA-sponsored Jet Propulsion Laboratory (JPL), California Institute of Technology. All the climate model simulate output used for this research can be downloaded from this website (http://web.gps.caltech.edu/~yzw/share/Wang-2020-JGR-Ice/). The code of NCAR CESM model used in this study is available at this site (http://www2.mmm.ucar.edu/wrf/users/download/get_source.html). We also acknowledge high-performance computing support from Pleiades provided at NASA Ames. All requests for materials in this paper should be addressed to Yuan Wang (yuan.wang@caltech.edu).

References

Eidhammer, T., Morrison, H., Bansemer, A., Gettelman, A., & Heymsfield, A. J. (2014). Comparison of ice cloud properties simulated by the Community Atmosphere Model (CAM5) with in-situ observations. *Atmospheric Chemistry and Physics*, *14*(18), 10,103–10,118. https://doi.org/10.5194/acp-14-10103-2014

Errico, R. M., Yang, R., Privé, N., Tai, K.-S., Todling, R., Sienkiewicz, M., & Guo, J. (2013). Development and validation of observing-system simulation experiments at NASA's Global modeling and Assimilation Office. *Quarterly Journal of the Royal Meteorological Society*, *139*, 1162–1178. https://doi.org/10.1002/qj2027

Fu, Q., & Liou, K. N. (1993). Parameterization of the radiative properties of cirrus clouds. *Journal of the Atmospheric Sciences*, *50*(13), 2008–2025.

Gettelman, A., Hannay, C., Bacmeister, J. T., Neale, R. B., Pendergrass, A. G., Danabasoglu, G., et al. (2019). High climate sensitivity in the Community Earth System Model version 2 (CESM2). *Geophysical Research Letters*, *46*, 8329–8337. https://doi.org/10.1029/2019GL083978

Gettelman, A., Morrison, H., & Ghan, S. J. (2008). A new two-moment bulk stratiform cloud microphysics scheme in the Community Atmosphere Model, version 3 (CAM3). Part II: Single-column and global results. *Journal of Climate*, *21*(15), 3660–3679. https://doi.org/10.1175/2008jcli2116.1

Hartmann, D. L., Gasparini, B., Berry, S. E., & Blossey, P. N. (2018). The life cycle and net radiative effect of tropical anvil clouds. *Journal of Advances in Modeling Earth Systems*, *10*, 3012–3029. https://doi.org/10.1029/2018MS001484

Jiang, J. H., Yue, Q., Su, H., Kangaslahti, P., Lebsock, M., Reising, S., et al. (2019). Simulation of remote sensing of clouds and humidity from space using a combined platform of radar and multifrequency microwave radiometers. *Earth and Space Science*, *6*, 1234–1243. https://doi.org/10.1029/2019EA000580

Jiang, J. H., Yue, Q., Su, H., Reising, S. C., Kangaslahti, P. P., Deal, W. R., et al. (2017). A simulation of ice cloud particle size, humidity, and temperature measurements from the TWICE CubeSat. *Earth and Space Science*, *4*(8), 574–587. https://doi.org/10.1002/2017EA000296

Kahn, B. H., Schreier, M. M., Yue, Q., Fetzer, E. J., Irion, F. W., Platnick, S., et al. (2015). Pixel-scale assessment and uncertainty analysis of AIRS and MODIS ice cloud optical thickness and effective radius. *Journal of Geophysical Research: Atmospheres*, *120*, 11,669–11,689. https://doi.org/10.1002/2015JD023950

Lai, R., Teng, S., Yi, B., Letu, H., Min, M., Tang, S., & Liu, C. (2019). Comparison of clouds properties from Hamawari-8 and FengYun-4A geostationary satellite radiometers with MODIS cloud retrievals. *Remote Sensing*, *11*, 1703. https://doi.org/10.3390/rs11141703

Li, G., Wang, Y., & Zhang, R. (2008). Implementation of a two-moment bulk microphysics scheme to the WRF model to investigate aerosol-cloud interaction. *Journal of Geophysical Research*, *113*, D15211. https://doi.org/10.1029/2007JD009361

Li, J. L. F., Lee, W.-L., Waliser, D., Wang, Y.-H., Yu, J.-Y., Jiang, X., et al. (2016). Considering the radiative effects of snow on tropical Pacific Ocean radiative heating profiles in contemporary GCMs using A-Train observations. *Journal of Geophysical Research: Atmospheres*, *121*, 1621–1636. https://doi.org/10.1002/2015JD023587

Li, J. L. F., Richardson, M., Hong, Y., Lee, W.-L., Wang, Y.-H., Yu, J.-Y., et al. (2017). Improved simulation of Antarctic sea ice due to the radiative effects of falling snow. *Environmental Research Letters*, *12*(8). https://doi.org/10.1088/1748-9326/aa7a17

Liu, C., Yang, P., Minnis, P., Loeb, N., Kato, S., Heymsfield, A., & Schmitt, C. (2014). A two-habit model for the microphysical and optical properties of ice clouds. *Atmospheric Chemistry and Physics*, *14*, 13,719–13,737. https://doi.org/10.5194/acp-14-13719-2014

Mitchell, D. L., Rasch, P., Ivanova, D., McFarquhar, G., & Nousiainen, T. (2008). Impact of small ice crystal assumptions on ice sedimentation rates in cirrus clouds and GCM simulations. *Geophysical Research Letters*, *35*, L09806. https://doi.org/10.1029/2008GL033552

Muri, H., Kristjánsson, J. E., Storelvmo, T., & Pfeffer, M. A. (2014). The climatic effects of modifying cirrus clouds in a climate engineering framework. *Journal of Geophysical Research: Atmospheres*, *119*, 4174–4191. https://doi.org/10.1002/2013JD021063

Qian, Y., Yan, H., Hou, Z., Johannesson, G., Klein, S., Lucas, D., et al. (2015). Parametric sensitivity analysis of precipitation at global and local scales in the Community Atmosphere Model CAM5. *Journal of Advances in Modeling Earth Systems*, *7*, 382–411. https://doi.org/10.1002/2014MS000354

Sanderson, B. M., Piani, C., Ingram, W. J., Stone, D. A., & Allen, M. R. (2007). Towards constraining climate sensitivity by linear analysis of feedback patterns in thousands of perturbed-physics GCM simulations. *Climate Dynamics*, *30*(2–3), 175–190. https://doi.org/10.1007/s00382-007-0280-7

Schiro, K., Su, H., Wang, Y., Langenbrunner, B., Jiang, J., & Neelin, J. D. (2019). Relationships between tropical ascent and high cloud fraction changes with warming revealed by perturbation physics experiments in CESM. *Geophysical Research Letters*, *46*, 10,112–10,121. https://doi.org/10.1029/2019GL083026

Schneider, T., Bischoff, T., & Haug, G. H. (2014). Migrations and dynamics of the intertropical convergence zone. *Nature*, *513*(7516), 45–53. https://doi.org/10.1038/nature13636

Stephens, G. L., Vane, D. G., Boain, R. J., Mace, G. G., Sassen, K., Wang, Z., et al., & the CloudSat Science Team (2002). The CloudSat mission and the A-Train—A new dimension of space-based observations of clouds and precipitation. *Bulletin of the American Meteorological Society*, *83*(12), 1771–1790. https://doi.org/10.1175/BAMS-83-12-1771

Stubenrauch, C. J., Rossow, W. B., Kinne, S., Ackerman, S., Cesana, G., Chepfer, H., et al. (2013). Assessment of global cloud datasets from satellites: Project and database initiated by the GEWEX radiation panel. *Bulletin of the American Meteorological Society*, *94*(7), 1031–1049. https://doi.org/10.1175/BAMS-D-12-00117.1

Su, H., Jiang, J. H., Neelin, J. D., Shen, T. J., Zhai, C., Yue, Q., et al. (2017). Tightening of tropical ascent and high clouds key to precipitation change in a warmer climate. *Nature Communications*, *8*(1), 15771. https://doi.org/10.1038/ncomms15771

Tan, I., Storelvmo, T., & Zelinka, M. D. (2016). Observational constraints on mixed-phase clouds imply higher climate sensitivity. *Science*, *352*(6282), 224–227.

Wang, C., Platnick, S., Fauchez, T., Meyer, K., Zhang, Z., Iwabuchi, H., & Kahn, B. H. (2019). An assessment of the impacts of cloud vertical heterogeneity on global ice cloud data records from passive satellite retrievals. *Journal of Geophysical Research: Atmospheres*, *124*, 1578–1595. https://doi.org/10.1029/2018JD029681

Wang, Y., Su, H., Jiang, J. H., Livesey, N. J., Santee, M. L., Froidevaux, L., et al. (2017). The linkage between stratospheric water vapor and surface temperature in an observation-constrained coupled general circulation model. *Climate Dynamics*, *48*(7–8), 2671–2683. https://doi.org/10.1007/s00382-016-3231-3

Yang, P., Liou, K. N., Bi, L., Liu, C., Yi, B., & Baum, B. A. (2015). On the radiative properties of ice clouds: light scattering, remote sensing and radiation parameterization. *Advances in Atmospheric Sciences*, *32*, 32–63. https://doi.org/10.1007/s00376-014-0011-z

Zhang, G. J., & Mcfarlane, N. A. (1995). Sensitivity of climate simulations to the parameterization of cumulus convection in the Canadian Climate Center General-Circulation Model. *Atmosphere-Ocean*, *33*(3), 407–446.

Zhao, B., Wang, Y., Gu, Y., Liou, K. N., Jiang, J. H., Fan, J., et al. (2019). Ice nucleation by aerosols from anthropogenic pollution. *Nature Geoscience*, *12*, 602–607. https://doi.org/10.1038/s41561-019-0389-4

Zhao, B., Zheng, H., Wang, S., Smith, K. R., Lu, X., Aunan, K., et al. (2018). Change in household fuels dominates the decrease in $PM_{2.5}$ exposure and premature mortality in China in 2005–2015. *Proceedings of the National Academy of Sciences of the United States of America*, *115*(49), 12,401–12,406. https://doi.org/10.1073/pnas.1812955115